

# Randomized 3D Scene Generation for Generalizable Self-supervised Pre-training

Lanxiao Li  
lanxiao.li@kit.edu

Michael Heizmann  
michael.heizmann@kit.edu

Institute of Industrial Information  
Technology (IIT)  
Karlsruhe Institute of Technology  
Karlsruhe, Germany

## Abstract

Capturing and labeling real-world 3D data is laborious and time-consuming, which makes it costly to train strong 3D models. To address this issue, previous works generate randomized 3D scenes and pre-train models on generated data. Although the pre-trained models gain promising performance boosts, previous works have two major shortcomings. First, they focus on only one downstream task (*i.e.*, object detection). Second, a fair comparison of generated data is still lacking. In this work, we systematically compare data generation methods using a unified setup. To clarify the generalization of the pre-trained models, we evaluate their performance in multiple tasks (*e.g.*, object detection and semantic segmentation) and with different pre-training methods (*e.g.*, masked autoencoder and contrastive learning). Moreover, we propose a new method to generate 3D scenes with spherical harmonics. It surpasses the previous formula-driven method with a clear margin and achieves on-par results with methods using real-world scans and CAD models.

## Introduction

Deep neural networks are data-hungry, whereas capturing and labeling data requires much time and human effort. This problem is especially concerning in 3D computer vision, as 3D data and labels are more scarce and expensive. To train strong 3D neural networks with lower costs, many works apply synthetic data in pre-training and fine-tune the models on real-world data. One possible approach for generating synthetic data is simulation [5, 9, 14, 32]. Although realistic scenes can be simulated, developing the simulation environment, crafting the source materials, and designing scene layouts still require a lot of effort. Recently, randomized 3D scene generation [26, 37] has shown promising results. This approach generates 3D scenes by randomly placing ‘objects’, which can be either CAD models [26] or formula-driven shapes [37], based on pre-defined rules. Randomized 3D scene generation requires neither real-world data nor manual annotation. Also, it saves effort in designing the scene layouts. However, previous works [26, 37] have two major issues. First, their pre-training methods are task-specific. Specifically, they are only designed for and evaluated on object detection, which limits their application to other tasks. Moreover, since they use different pretext tasks for pre-training, the contribution of the generated data is not clear. A fair comparison of different data-generating methods is still missing.

For a better understanding and application of randomized 3D scene generation in 3D computer vision, it’s important to compare previous methods under a fair setup. Also, to pre-train models which can generalize on different downstream tasks, it’s necessary to apply

a general pre-training approach instead of task-specific ones. In this work, we choose masked autoencoder (MAE) [14] and contrastive learning [4, 14] to pre-train models, as they generalize well on multiple tasks and show an impressive performance in previous research. Our experimental results show that randomly generated 3D scenes bring on-par improvement as real-world data. Also, the pre-trained models generalize well on different downstream tasks, *e.g.*, object detection and semantic segmentation.

Also, using formula-driven shapes, *e.g.*, fractal point clouds [57], instead of CAD models for scene generation, is more promising since it doesn't rely on additional data. However, we empirically find that fractal point clouds show sub-optimal results in pre-training. Since real-world 3D data are usually captured with depth sensors (*e.g.*, laser scanners or RGB-D cameras), which cannot measure the internal structure of objects, real-world data only contain sample points on object surfaces. Our intuition is that the objects used for scene generation should contain sufficient surfaces so that the pre-trained models can be transferred to downstream tasks with real-world data. Fractal point clouds, on the contrary, don't contain continuous surfaces (see Fig. 2). We hypothesize that this domain gap makes the pre-training less effective.

To solve this problem, we propose to use spherical harmonics, which are formula-driven with natural surfaces, as objects for randomized 3D scene generation. Experimental results show that spherical harmonics outperform fractal point clouds with a clear margin and are competitive compared to CAD models and even real-world data in pre-training.

The contribution of this work is many-fold: (1) our work, for the first time, explores generalizable pre-training using randomized scene generation and systematically compares the generated data in multiple tasks. (2) our experiments provide a deeper understanding of randomized 3D scene generation, *e.g.*, the impact of object sets and view angles. (3) we propose to generate scenes with formula-driven spherical harmonics and achieve competitive results in 3D object detection and semantic segmentation without using real-world data or CAD models in the pre-training stage.

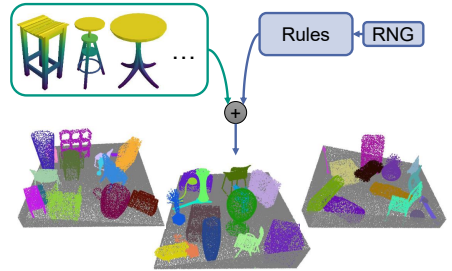


Figure 1: Concept of randomized 3D scene generation. Key components: an object set and generation rules. RNG: random number generator.

## 2 Related Works

**Self-supervised Pre-training for 3D Vision.** A lot of methods utilize the invariance of 3D features to establish correspondence between different views and apply contrastive learning [13, 16, 35, 36, 40]. Also, some works transfer knowledge from other domains, *e.g.*, color images [25] and language [40]. Moreover, some works [8, 31, 33] reconstruct partially visual point clouds in the pretext task. Recent works [17, 18, 27, 39] apply the successful masked autoencoder [14] on point clouds.

**Simulation-based Scene Generation.** Deschaud *et al.* [6] employ CARLA simulator [6] and generate synthetic LiDAR point clouds for 3D mapping tasks. Griffiths and Boehm [9] present a large-scale point cloud of the urban environment using BlenSor [10]. Xiao *et al.* [34] collect point cloud data using Unreal Engine 4 (UE4) and investigate the transfer

learning from synthetic to real-world data in semantic segmentation. Wu *et al.* [32] and Hurl *et al.* [14] synthesize training data using Grand Theft Auto V, a popular video game.

**Randomized Scene Generation.** Rao *et al.* [26] generate scenes by randomly placing CAD models in randomly created rooms. They create pairs of scenes with the same objects but different layouts and perform contrastive learning using object-level correspondence. Yamada *et al.* [57] employ fractal point clouds as objects instead of CAD models. They generate bounding box labels for each object and pre-train object detectors in a fully supervised manner. Both methods are only evaluated in object detection tasks.

## 3 Method

### 3.1 Concept of Randomized 3D Scene Generation

As shown in Fig. 1, randomized 3D scene generation requires an object set and pre-defined rules. A room with a random size is first created to generate a new scene. A 3D object is randomly picked from the set, undergoes data augmentation (*e.g.*, rotation and scaling), and is randomly placed in the room. The process is repeated until the room contains enough objects. The rules define *e.g.*, the distribution of room size, choices and parameters for data augmentation, distribution of objects in the room, and the number of objects in each scene. With an object set and rules are given, a vast amount scenes can be easily generated.



Figure 2: Examples of objects used for scene generation. Left: CAD models from ModelNet40 [53]. Middle: fractal point clouds [57]. Right: spherical harmonics. Some objects are shown as meshes, although only sampled points are used for pre-training.

Previous works use similar rules while having different choices on object sets. Rao *et al.* [26] use CAD models, which is straightforward since openly accessible datasets of CAD models are commonly used in 3D computer vision [4, 53]. This choice has the drawback that creating or gathering CAD models is still laborious and time-consuming. On the contrary, Yamada *et al.* [57] propose generating the object sets in a randomized manner. Specifically, they create fractal point clouds by randomly sampling affine transformations and iteratively applying them to 3D points. However, we hypothesize this method is sub-optimal as the fractal point clouds don’t have surfaces (see Fig. 2) and lead to a domain gap.

### 3.2 Objects and Scenes

**Spherical Harmonics.** In this work, we propose to generate object sets using spherical harmonics, which can be represented in a spherical coordinate system  $(r, \theta, \phi)$ :

$$r = \sin(m_1\phi)^{p_1} + \cos(m_2\phi)^{p_2} + \sin(m_3\theta)^{p_3} + \cos(m_4\theta)^{p_4}, \quad (1)$$

where  $m_i \in \mathbb{R}$  and  $p_i \in \mathbb{Z}^*$  with  $i \in \{1, 2, 3, 4\}$ . With fixed coefficients  $m_i$  and  $p_i$ , Eq. 1 describes a closed surface in 3D space. Diverse 3D objects can be generated when the coefficients are randomly set. Some spherical harmonics are visualized in Fig. 2. The spherical

harmonics are originally employed to solve partial differential equations [20]. In computer vision, they are also applied to describe surfaces and shapes [15, 21]. The form in Eq. 1 is motivated by the original definition but doesn't strictly follow it. In this work, the mathematical and physical meanings of spherical harmonics are not considered, and we solely utilize them to parameterize the object set. The idea is also inspired by a web page written by Paul Bourke<sup>1</sup>. Notice that the generated spherical harmonics can be easily represented as (rectangular) meshes, when coordinates  $\phi$  and  $\theta$  are sampled with constant intervals. The mesh representation greatly simplifies further processing, *e.g.*, point sampling and ray-casting (explained later in this subsection).

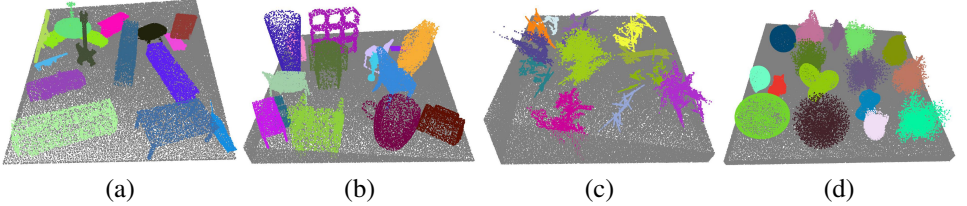


Figure 3: Examples of generated 3D scenes in point cloud representation. From left to right: using CAD models from ShapeNetCore [2], CAD models from ModelNet40 [53], fractal point clouds, and spherical harmonics, respectively. The colors here are solely for visualization purposes. The generated synthetic point clouds don't contain color channels.

**From Objects to Scenes.** We assume all scenes are static, following previous works. Also, we only consider downstream tasks in indoor scenes, while extending the methods to outdoor scenarios is straightforward. We adopt the generation rules of Rao *et al.* [26] and represent generated 3D scenes as point clouds. For each randomly picked object, we normalize it into a unit sphere, randomly sample 3000 points, and apply random data augmentation. Each generated scene contains 12 to 16 objects. Since random scaling is used as data augmentation, the point density on each object might differ. To create a point cloud with consistent density, we further apply grid sampling with the voxel size of 0.04 m. The generated scenes are visualized in Fig. 3. Our data generation process is simpler than previous works [26, 57] since we only generate single point clouds independently (*cf.* Sec. 2).

**Single-View Data.** Previous works represent the generated scenes as multi-view point clouds. In this work, a point cloud is referred to as multi-view when it cannot be projected to one surface without information loss. A typical example of multi-view point clouds is a 3D scan reconstructed from data sequences. On the contrary, many point clouds in practice are single-view and represented as depth maps (*e.g.*, from depth cameras) or range images (*e.g.*, from rotational laser scanners). Besides comparing different methods for randomized scene generation, it's also meaningful to compare the synthetic data with real-world ones. A lot of works use single-view real-world data for self-supervised pre-training [13, 16, 35, 36, 40], since they are the direct output from sensors and easy to obtain. To clarify the impact of single-view and multi-view representations in pre-training and for a fairer comparison with the real-world data, we also generate single-view point clouds in this work. We create scenes using meshes as objects instead of sampled point clouds but still following the same rules in [26]. Then, we set a virtual camera with a random pose and capture a depth map using ray-casting. The camera pose is checked so that each depth map contains sufficient objects (set to 7 in this work). In pre-training, the depth maps are converted into point clouds on the

<sup>1</sup><http://paulbourke.net/geometry/sphericalh/>. Last access on 2023.4.3.

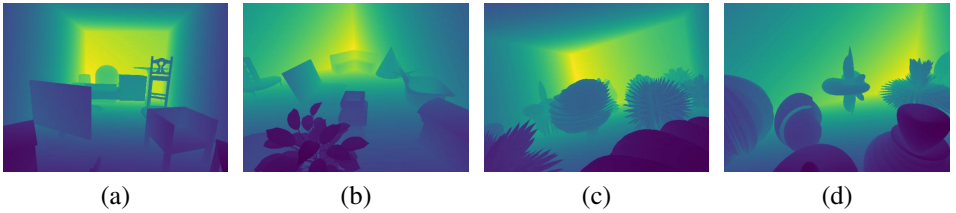


Figure 4: Examples of generated depth maps via ray-casting. (a): with objects from ShapeNetCore [2]. (b): with objects from ModelNet40 [33]. (c) and (d): with spherical harmonics. According to the rules in [26], objects might be stacked on others.

flight. Some generated depth maps are visualized in Fig. 4. We don’t generate depth maps with fractal point clouds since ray-casting is non-trivial in this case.

### 3.3 Self-supervised Pre-training

In this work, we explore the generalizable pre-training using generated synthetic data. Instead of using a pre-training strategy specific to one downstream task, we apply masked autoencoder (MAE) [14] and MoCoV2 [9], a successful method for contrastive learning, to evaluate the generated data. In this subsection, we briefly introduce the concept of the two pre-training methods.

MAE [14] is employed to pre-train vision transformers [2, 30]. An input point cloud is divided into small patches, and a large proportion is masked. A transformer encoder extracts patch-wise features from the remaining patches, and a transformer decoder is trained to reconstruct the masked patches. After the pre-training, the decoder is abandoned, and the encoder can be transferred into downstream tasks. In this work, we adopt the method of Li and Heizmann [14] for MAE. Also, to increase the diversity of training data, we randomly crop a region from a generated scene in each iteration instead of using the entire scene.

We pre-train a point cloud encoder using scene-level contrastive learning following [14]. Specifically, we randomly crop two overlapping regions from each generated scene to create a positive pair. Point clouds from different scenes are considered negative samples. Given a point cloud, the encoder is trained to distinguish its positive sample from many negative samples. We apply MoCoV2 [9] by using an exponentially moving averaged momentum encoder and a memory bank to save global features from negative samples.

## 4 Experiments

### 4.1 Setup

**Real-World Baseline.** To create a baseline using real-world data, we pre-train our models on ScanNet [8], a large-scale indoor dataset of 2M RGB-D frames captured in 1500 rooms. We sample 78K frames (approximately one in every 25 frames or one per second) from the raw data in the training set, following previous works [14, 16, 35].

**Scene Generation.** To evaluate the impact of different object sets, we generate data with four object sets, summarized in Tab. 1. For CAD models, we use ShapeNetCore [2] and ModelNet40 [33]. The former consists of  $\sim 50$ K models of ordinary everyday objects (*e.g.*, chairs and shelves), while the latter contains  $\sim 10$ K. We follow their official train/val split

and use only objects from training sets. In our default setup, we create 10K formula-driven 3D objects to align the object number with ModelNet40. For fractal point clouds, we follow the configuration of Yamada *et al.* [57]. We generate 78K scenes with each object set in our default setup, following the real-world baseline. We name the generated datasets RM-ShapeNet, RM-ModelNet, RM-Fractal, and RM-Harmonics according to object sets. The abbreviation RM stands for RandomRooms [26], as we adopt its generation rules.

**Masked Autoencoder.** We use the same architecture as [17]. A 3-layer transformer encoder [50] extracts features from input patches. A decoder with 2 layers is attached to the encoder for pre-training with MAE. We follow the configuration in [17] and train all models for 120 epochs with a batch size of 64 and an AdamW optimizer. We evaluate the pre-trained point cloud transformer for 3D object detection on ScanNet [9] benchmark. We use 3DETR [19] as the detection head and fine-tune the model for 1080 epochs with batch size 8, following the original setup. Mean average precision with a 3D IoU threshold of 25% and 50% (*i.e.*, AP25 and AP50) over 18 classes are evaluation matrices. We also fine-tune the pre-trained transformer for semantic segmentation on S3DIS [10] dataset. We use the same segmentation head and protocol as [17] and train for 300 epochs with batch size 12. We report mean accuracy (mAcc) and mean IoU (mIoU) over 13 classes in Area 5.

**Contrastive Learning.** We train a PointNet++ [23] for contrastive learning, following previous works [16, 26, 57, 40]. The network architecture is adopted from [24], which consists of 4 Set Abstraction modules [23] and 2 Feature Propagation modules [23]. We use MoCoV2 to pre-train the model. Specifically, we apply a global max-pooling and 3 fully connected layers to encode the features from PointNet++. Momentum of the momentum encoder is set to 0.999, and the size of the memory bank is 24576. We train for 120 epochs using an SGD optimizer, an initial learning rate of 0.01, a batch size of 12, and a cosine annealing schedule. After pre-training, we initialize a VoteNet [24] with the pre-trained model and fine-tune it for 3D object detection on ScanNet [9] and SUN RGB-D [28] benchmark. The SUN RGB-D dataset consists of  $\sim 10$ K point clouds, with half for training and half for validation. AP25 and AP50 are calculated over 10 representative classes. We apply the original configuration of VoteNet for fine-tuning. Each model is trained for 180 epochs, a batch size of 8, and a learning rate of 0.001, decayed with a factor of 0.1 after 120, 140, and 160 epochs, respectively.

More technical details are provided in our supplementary materials.

## 4.2 Experimental Results

**Mask Autoencoder.** We pre-train an MAE with generated data and report the fine-tuning performance in Tab. 2. Compared to results without pre-training (row 1), all pre-trained models gain a significant improvement in object detection and semantic segmentation.

Among multi-view variants of randomly generated data (row 3 to 6), using ShapeNet as object set (RM-ShapeNet) delivers the best performance since ShapeNet is significantly larger than other object sets (see Tab. 1). Meanwhile, RM-Fractal brings the least improvement. It verifies our intuition that fractal point clouds as objects are non-optimal in data generation due to lack of surface. Interestingly, with the same object number, RM-Harmonics

Dataset	Obj. Set	Obj. Num.
RM-ShapeNet	ShapeNetCore [9]	$\sim 50$ K
RM-ModelNet	ModelNet40 [53]	$\sim 10$ K
RM-Fractal	Fractal Points [57]	10K
RM-Harmonics	Spherical Harmonics	10K

Table 1: Summary of generated datasets.



Dataset	View	Det.		Seg.	
		AP25	AP50	mAcc	mIoU
Scratch [14]	-	61.6	38.8	66.4	60.0
ScanNet [14]	single	64.1	43.0	74.7	67.6
RM-ShapeNet	multi	63.8	42.6	74.6	67.8
RM-ModelNet	multi	63.5	42.0	73.6	67.0
RM-Fractal	multi	62.8	40.4	70.2	64.1
RM-Harmonics	multi	63.8	43.2	74.1	67.1
RM-ShapeNet	single	63.8	42.9	73.8	67.2
RM-ModelNet	single	62.5	41.6	73.5	66.3
RM-Harmonics	single	63.5	42.1	73.5	67.1

Table 2: Downstream task performance of an MAE pre-trained on different datasets. Detection results are on the ScanNet detection benchmark. Segmentation results are on S3DIS dataset. The first and second columns refer to the pre-training data. All metrics in percentage.

Dataset	View	SUN RGB-D		ScanNet	
		AP25	AP50	AP25	AP50
Scratch [14]	-	58.4	33.3	60.0	37.6
ScanNet	single	60.8	35.7	62.2	39.0
RM-ShapeNet	multi	59.8	34.1	62.7	37.9
RM-ModelNet	multi	59.3	33.7	62.3	37.3
RM-Fractal	multi	59.1	33.4	61.3	38.6
RM-Harmonics	multi	59.6	35.7	62.6	39.7
RM-ShapeNet	single	58.9	33.0	64.1	40.0
RM-ModelNet	single	57.9	32.4	63.4	39.8
RM-Harmonics	single	58.6	33.1	63.5	39.8
Rao <i>et al.</i> [14]	multi	59.2	-	61.3	-
Yamada <i>et al.</i> [14]	multi	59.4	33.9	61.9	38.3

Table 3: Fine-tuning results of contrastive learning using generated data. Evaluation for 3D object detection on SUN RGB-D and ScanNet benchmark. All metrics in percentage.

outperform RM-ModelNet. The result is promising since it implies that randomly generated objects can replace CAD models for scene generation. However, most CAD models in ModelNet40 are ordinary objects in daily life, *e.g.*, chairs and tables, while both datasets in downstream tasks are captured in indoor environments, *e.g.*, living rooms and offices. One should expect ModelNet40 to perform better than spherical harmonics because of the similarity between pre-training and fine-tuning data. We believe this contradiction is caused by the diversity of the object set. Although ModelNet40 contains 40 classes, the appearance of the objects in the same class is similar. Also, the class distribution in ModelNet40 is long-tailed, which might also have a negative impact [14]. On the other hand, spherical harmonics are generated by uniformly sampling the coefficients, which results in a more diverse and balanced object set. Furthermore, we compare the results of generated synthetic data with the real-world ScanNet dataset (row 2). With the same number of point clouds, The performance of RM-ShapeNet and RM-Harmonics is close to real-world data, demonstrating the effectiveness of randomized scene generation in self-supervised training.

With generated single-view data (*i.e.*, depth maps), a similar trend can also be observed: RM-ShapeNet performs the best, while RM-Harmonics is more effective than RM-ModelNet. Data generation with fractal points is not performed since ray-casting relies on mesh data. However, compared to their corresponding multi-view variants, all single-view datasets perform worse with MAE.

**Contrastive Learning.** For contrastive learning, we pre-train a PointNet++ using MoCoV2 and fine-tune a VoteNet using it as the backbone. Object detection results on ScanNet and SUN RGB-D are reported in Tab. 3. Generally, pre-trained models achieve better detection quality than the baseline without pre-training on both benchmarks. For the multi-view datasets (row 3 to 6), RM-ShapeNet and RM-Harmonics show on-par performance. RM-ModelNet performs worse than these two datasets, while RM-Fractal brings the smallest improvement in pre-training. Compared to real-world data (ScanNet), randomly generated data shows significantly worse results on SUN RGB-D dataset, while the gap disappears on the ScanNet detection benchmark.

The relative performance of single-view variants of generated data is similar to the multi-

view ones, *e.g.*, RM-ShapeNet > RM-Harmonic > RM-ModelNet. However, the detection results on SUN RGB-D dataset are worse than with multi-view data. On the contrary, single-view datasets show significantly better results on the ScanNet benchmark. This observation is counter-intuitive. Notice that SUN RGB-D consists of single-view point clouds, whereas the ScanNet benchmark applies point clouds reconstructed from multi-views. One should expect that models pre-trained using single-view data perform worse on the ScanNet benchmark due to the domain gap. The reason for the observation is not fully understood. However, it must be correlated with the pre-training schema since it's not observed with MAE.

We also compare our results with two previous works on randomized 3D scene generation, *e.g.*, RandomRooms [26] and PC-FractalDB [57], each of which applies a training strategy specialized for object detection. Both methods use VoteNet as the detector and apply a PointNet++ as the backbone. Our model pre-trained with RM-Fractal achieves similar performance as the method of Yamada *et al.* [57], which also generates scenes using fractal point clouds. Also, our RM-Harmonics (multi-view) outperforms both previous works by a clear margin. It shows that the choice of object sets has a larger impact than pre-training methods. Also, it implies that a task-specific design is unnecessary in pre-training and general purpose methods (*e.g.*, MAE and MoCoV2) are sufficient.

**Main Results and Discussions.** The experimental results in Tab. 2 and 3 can be summarized as follows: (1) Randomized scene generation is effective for pre-training 3D models with self-supervision. This approach generalizes well across different pre-training methods and downstream tasks. Also, its performance is comparable with real-world data. (2) Formula-driven spherical harmonics perform significantly better than fractal point clouds and achieve on-par results as hand-crafted CAD models. (3) The diversity of objects greatly impacts the effect of pre-training. An object set with a larger diversity is generally beneficial. (4) Single-view and multi-view variants of generated data bring different results. However, the impact is inconsistent across different pre-training methods and fine-tuning datasets.

The observation that randomly generated data have a similar effect as real-world ones in self-supervised pre-training is interesting since they don't look photo-realistic (see Fig. 3), especially when formula-driven objects are applied. We believe it's because neural networks perform different tasks in self-supervised pre-training and fine-tuning (*i.e.*, pre-training and downstream tasks are decoupled). Therefore, the performance in fine-tuning is not sensitive to the domain gap between pre-training and fine-tuning data. However, a too large gap can still significantly harm the performance, *e.g.*, fractal point clouds without surfaces perform worse than spherical harmonics in our experiments.

**Comparison with other Pre-training Methods.** We also compare the fine-tuning performance of our models pre-trained on RM-Harmonics with other pre-training methods in Tab. 4. All methods indicated with 'real' are pre-trained on real-world data from ScanNet, while DepthContrast† in Tab. 4 also uses data from the larger Redwood indoor RGB-D scan dataset [27]. All methods in the upper half of Tab. 4 fine-tune a VoteNet with a pre-trained PointNet++ as the backbone, while methods in the lower half use a 3DETR with a pre-trained transformer. Compared with methods using real-world data for pre-training, our methods achieve competitive performance. However, our pre-training data are randomly generated and require neither real-world 3D scans nor hand-crafted CAD models.

**Object and Scene Numbers.** In this work, we propose generating scenes using spherical harmonics as objects. In this experiment, we investigate the impact of object and scene numbers. We first fix the number of used spherical harmonics in scene generation (*i.e.*, 10K) and scale the scene number. As shown in the upper half of Tab. 5, using more scenes in pre-training is generally beneficial. But there is no significant improvement when more than



Methods	Data	Model	AP25	AP50
VoteNet [24]	-	P	60.0	37.6
Hou <i>et al.</i> [13]	real	P	-	39.3
DepthContrast [10]	real	P	61.3	-
DepthContrast <sup>†</sup> [10]	real	P	64.0	42.9
DPCo [16]	real	P	64.2	41.5
Rao <i>et al.</i> [26]	syn.	P	61.3	-
Yamada <i>et al.</i> [6]	syn.	P	61.9	38.3
Ours (multi-view)	syn.	P	62.6	39.7
Ours (single-view)	syn.	P	63.5	39.8
3DETR [19]	-	T	62.1	37.9
MaskPoint (L3) [18]	real	T	63.4	40.6
MaskPoint (L12) [18]	real	T	64.2	42.1
Li & Heizmann [14]	real	T	64.1	43.0
Ours (multi-view)	syn.	T	63.8	43.2
Ours (single-view)	syn.	T	63.5	42.1

Objects	Scenes	AP25	AP50
-	-	61.6	38.8
×1	×0.2	62.9	41.1
×1	×0.5	63.5	42.7
×1	×1	63.8	43.2
×1	×2	63.8	43.4
×1	×5	63.4	42.9
×0.2	×1	62.4	41.8
×0.5	×1	63.9	42.8
×1	×1	63.8	43.2
×2	×1	63.2	41.7
×5	×1	62.5	40.6
×2	×2	63.2	42.5
×5	×5	63.0	42.2

Table 4: Object detection results on ScanNet detection benchmark. Data: type of pre-training data (real-world, synthetic or none). Model: the architecture of backbones. P: PointNet++, T: transformer.

Table 5: Impact of object and scene numbers. Multi-view point clouds with spherical harmonics. Evaluated for object detection on ScanNet. ×1: 10K objects or 78K scenes, respectively. ×*a*: scaling with factor *a*.

78K scenes (×1) are applied.

Furthermore, we fix the scene number to our default value and scale the object number. With a small object number (×0.2), the generated scenes have a smaller diversity, which harms the effect of pre-training. However, a large object number (×5) also produces significantly worse results. Also, scaling up the scene number and object number simultaneously (the last two rows) doesn’t bring improvement, compared to the default setup. We hypothesize it’s due to the limited diversity of spherical harmonics described by Eq. 1. Since the equation has only 8 free coefficients, with a too large object number, the minimal ‘distance’ between generated objects becomes smaller<sup>2</sup>. As a result, some generated scenes contain very similar objects, which has a negative impact on pre-training. Based on the discussion, searching for new formulas with more degrees of freedom is beneficial. We leave the exploration to future works.

## 5 Conclusion

This work demonstrates the power of randomized 3D scene generation in self-supervised pre-training. The generated data perform well with different pre-training methods, and the pre-trained models achieve impressive results in multiple downstream tasks. Also, we take a closer look at the impact of object sets and propose to replace CAD models with formula-driven spherical harmonics. The method is promising since it reduces pre-training costs without harming performance. We hope our work can inspire more research on randomized data generation for self-supervised pre-training.

<sup>2</sup>Consider the situation where  $n$  points in a continuous interval  $[0, 1]$  have to be independently and uniformly sampled. The minimal distance between two points decreases with increasing  $n$ .

## References

- [1] Iro Armeni, Sasha Sax, Amir Roshan Zamir, and Silvio Savarese. Joint 2d-3d-semantic data for indoor scene understanding. *CoRR*, abs/1702.01105, 2017.
- [2] Angel X. Chang, Thomas Funkhouser, Leonidas Guibas, Pat Hanrahan, Qixing Huang, Zimo Li, Silvio Savarese, Manolis Savva, Shuran Song, Hao Su, et al. ShapeNet: An information-rich 3D model repository. *arXiv preprint arXiv:1512.03012*, 2015.
- [3] Xinlei Chen, Haoqi Fan, Ross Girshick, and Kaiming He. Improved baselines with momentum contrastive learning. *arXiv preprint arXiv:2003.04297*, 2020.
- [4] Angela Dai, Angel X. Chang, Manolis Savva, Maciej Halber, Thomas Funkhouser, and Matthias Nießner. ScanNet: Richly-annotated 3D reconstructions of indoor scenes. In *Proceedings of the IEEE conference on computer vision and pattern recognition*, pages 5828–5839, 2017.
- [5] Jean-Emmanuel Deschaut, David Duque, Jean Pierre Richa, Santiago Velasco-Forero, Beatriz Marcotegui, and François Goulette. Paris-carla-3d: A real and synthetic outdoor point cloud dataset for challenging tasks in 3D mapping. *Remote Sensing*, 13(22): 4713, 2021.
- [6] Alexey Dosovitskiy, German Ros, Felipe Codevilla, Antonio Lopez, and Vladlen Koltun. CARLA: An open urban driving simulator. In *Proceedings of the 1st Annual Conference on Robot Learning*, pages 1–16, 2017.
- [7] Alexey Dosovitskiy, Lucas Beyer, Alexander Kolesnikov, Dirk Weissenborn, Xiaohua Zhai, Thomas Unterthiner, Mostafa Dehghani, Matthias Minderer, Georg Heigold, Sylvain Gelly, et al. An image is worth 16x16 words: Transformers for image recognition at scale. *arXiv preprint arXiv:2010.11929*, 2020.
- [8] Kexue Fu, Peng Gao, ShaoLei Liu, Renrui Zhang, Yu Qiao, and Manning Wang. POS-BERT: Point cloud one-stage BERT pre-training. *arXiv preprint arXiv:2204.00989*, 2022.
- [9] David Griffiths and Jan Boehm. SynthCity: A large scale synthetic point cloud. *arXiv preprint arXiv:1907.04758*, 2019.
- [10] Michael Gschwandtner, Roland Kwitt, Andreas Uhl, and Wolfgang Pree. BlenSor: Blender sensor simulation toolbox. In *Advances in Visual Computing: 7th International Symposium, ISVC 2011, Las Vegas, NV, USA, September 26-28, 2011. Proceedings, Part II* 7, pages 199–208. Springer, 2011.
- [11] Kaiming He, Haoqi Fan, Yuxin Wu, Saining Xie, and Ross Girshick. Momentum contrast for unsupervised visual representation learning. In *Proceedings of the IEEE/CVF conference on computer vision and pattern recognition*, pages 9729–9738, 2020.
- [12] Kaiming He, Xinlei Chen, Saining Xie, Yanghao Li, Piotr Dollár, and Ross Girshick. Masked autoencoders are scalable vision learners. In *Proceedings of the IEEE/CVF Conference on Computer Vision and Pattern Recognition*, pages 16000–16009, 2022.

- [13] Ji Hou, Benjamin Graham, Matthias Nießner, and Saining Xie. Exploring data-efficient 3D scene understanding with contrastive scene contexts. In *Proceedings of the IEEE/CVF Conference on Computer Vision and Pattern Recognition*, pages 15587–15597, 2021.
- [14] Braden Hurl, Krzysztof Czarnecki, and Steven Waslander. Precise synthetic image and lidar (presil) dataset for autonomous vehicle perception. In *2019 IEEE Intelligent Vehicles Symposium (IV)*, pages 2522–2529. IEEE, 2019.
- [15] Michael Kazhdan, Thomas Funkhouser, and Szymon Rusinkiewicz. Rotation invariant spherical harmonic representation of 3D shape descriptors. In *Symposium on geometry processing*, volume 6, pages 156–164, 2003.
- [16] Lanxiao Li and Michael Heizmann. A closer look at invariances in self-supervised pre-training for 3D vision. In *Computer Vision–ECCV 2022: 17th European Conference, Tel Aviv, Israel, October 23–27, 2022, Proceedings, Part XXX*, pages 656–673. Springer, 2022.
- [17] Lanxiao Li and Michael Heizmann. Applying plain transformers to real-world point clouds. *arXiv preprint arXiv:2303.00086*, 2023.
- [18] Haotian Liu, Mu Cai, and Yong Jae Lee. Masked discrimination for self-supervised learning on point clouds. *Proceedings of the European Conference on Computer Vision (ECCV)*, 2022.
- [19] Ishan Misra, Rohit Girdhar, and Armand Joulin. An end-to-end transformer model for 3D object detection. In *Proceedings of the IEEE/CVF International Conference on Computer Vision*, pages 2906–2917, 2021.
- [20] Claus Müller. *Spherical harmonics*, volume 17. Springer, 2006.
- [21] Yatian Pang, Wenxiao Wang, Francis EH Tay, Wei Liu, Yonghong Tian, and Li Yuan. Masked autoencoders for point cloud self-supervised learning. *ECCV*, 2022.
- [22] Jaesik Park, Qian-Yi Zhou, and Vladlen Koltun. Colored point cloud registration revisited. In *Proceedings of the IEEE international conference on computer vision*, pages 143–152, 2017.
- [23] Charles R. Qi, Li Yi, Hao Su, and Leonidas J. Guibas. PointNet++: Deep hierarchical feature learning on point sets in a metric space. *Advances in neural information processing systems*, 30, 2017.
- [24] Charles R. Qi, Or Litany, Kaiming He, and Leonidas J. Guibas. Deep Hough voting for 3D object detection in point clouds. In *proceedings of the IEEE/CVF International Conference on Computer Vision*, pages 9277–9286, 2019.
- [25] Guocheng Qian, Xingdi Zhang, Abdullah Hamdi, and Bernard Ghanem. Pix4Point: Image pretrained transformers for 3D point cloud understanding. *arXiv preprint arXiv:2208.12259*, 2022.

- [26] Yongming Rao, Benlin Liu, Yi Wei, Jiwen Lu, Cho-Jui Hsieh, and Jie Zhou. Randomrooms: unsupervised pre-training from synthetic shapes and randomized layouts for 3D object detection. In *Proceedings of the IEEE/CVF International Conference on Computer Vision*, pages 3283–3292, 2021.
- [27] Dietmar Saupe and Dejan V Vranić. 3D model retrieval with spherical harmonics and moments. In *Pattern Recognition: 23rd DAGM Symposium Munich, Germany, September 12–14, 2001 Proceedings 23*, pages 392–397. Springer, 2001.
- [28] Shuran Song, Samuel P. Lichtenberg, and Jianxiong Xiao. SUN RGB-D: A RGB-D scene understanding benchmark suite. In *Proceedings of the IEEE conference on computer vision and pattern recognition*, pages 567–576, 2015.
- [29] Yonglong Tian, Olivier J Henaff, and Aäron van den Oord. Divide and contrast: Self-supervised learning from uncurated data. In *Proceedings of the IEEE/CVF International Conference on Computer Vision*, pages 10063–10074, 2021.
- [30] Ashish Vaswani, Noam Shazeer, Niki Parmar, Jakob Uszkoreit, Llion Jones, Aidan N. Gomez, Łukasz Kaiser, and Illia Polosukhin. Attention is all you need. *Advances in neural information processing systems*, 30, 2017.
- [31] Hanchen Wang, Qi Liu, Xiangyu Yue, Joan Lasenby, and Matt J. Kusner. Unsupervised point cloud pre-training via occlusion completion. In *Proceedings of the IEEE/CVF international conference on computer vision*, pages 9782–9792, 2021.
- [32] Bichen Wu, Alvin Wan, Xiangyu Yue, and Kurt Keutzer. Squeezeseg: Convolutional neural nets with recurrent crf for real-time road-object segmentation from 3D lidar point cloud. In *2018 IEEE international conference on robotics and automation (ICRA)*, pages 1887–1893. IEEE, 2018.
- [33] Zhirong Wu, Shuran Song, Aditya Khosla, Fisher Yu, Linguang Zhang, Xiaoou Tang, and Jianxiong Xiao. 3D ShapeNets: A deep representation for volumetric shapes. In *Proceedings of the IEEE conference on computer vision and pattern recognition*, pages 1912–1920, 2015.
- [34] Aoran Xiao, Jiaying Huang, Dayan Guan, Fangneng Zhan, and Shijian Lu. Transfer learning from synthetic to real lidar point cloud for semantic segmentation. In *Proceedings of the AAAI Conference on Artificial Intelligence*, volume 36, pages 2795–2803, 2022.
- [35] Saining Xie, Jiatao Gu, Demi Guo, Charles R Qi, Leonidas Guibas, and Or Litany. PointContrast: Unsupervised pre-training for 3D point cloud understanding. In *Computer Vision—ECCV 2020: 16th European Conference, Glasgow, UK, August 23–28, 2020, Proceedings, Part III 16*, pages 574–591. Springer, 2020.
- [36] Chenfeng Xu, Shijia Yang, Bohan Zhai, Bichen Wu, Xiangyu Yue, Wei Zhan, Peter Vajda, Kurt Keutzer, and Masayoshi Tomizuka. Image2point: 3D point-cloud understanding with pretrained 2d convnets. *Proceedings of the European Conference on Computer Vision (ECCV)*, 2022.

- [37] Ryosuke Yamada, Hirokatsu Kataoka, Naoya Chiba, Yukiyasu Domae, and Tetsuya Ogata. Point cloud pre-training with natural 3D structures. In *Proceedings of the IEEE/CVF Conference on Computer Vision and Pattern Recognition*, pages 21283–21293, 2022.
- [38] Xumin Yu, Lulu Tang, Yongming Rao, Tiejun Huang, Jie Zhou, and Jiwen Lu. Point-BERT: Pre-training 3D point cloud transformers with masked point modeling. In *CVPR*, pages 19313–19322, 2022.
- [39] Renrui Zhang, Ziyu Guo, Peng Gao, Rongyao Fang, Bin Zhao, Dong Wang, Yu Qiao, and Hongsheng Li. Point-M2AE: Multi-scale masked autoencoders for hierarchical point cloud pre-training. *arXiv preprint arXiv:2205.14401*, 2022.
- [40] Renrui Zhang, Ziyu Guo, Wei Zhang, Kunchang Li, Xupeng Miao, Bin Cui, Yu Qiao, Peng Gao, and Hongsheng Li. PointCLIP: Point cloud understanding by CLIP. In *Proceedings of the IEEE/CVF Conference on Computer Vision and Pattern Recognition*, pages 8552–8562, 2022.
- [41] Zaiwei Zhang, Rohit Girdhar, Armand Joulin, and Ishan Misra. Self-supervised pre-training of 3D features on any point-cloud. In *Proceedings of the IEEE/CVF International Conference on Computer Vision*, pages 10252–10263, 2021.

## Appendix

### A Generating Spherical Harmonics

To generate sufficient objects for creating randomized scenes, we randomly set the coefficients in spherical harmonics. In this work, we constrain  $m_i$  in the range  $[-5, 5]$  and  $p_i$  in  $[0, 4]$ , since too large coefficients lead to high-frequency structures. Due to the sampling theorem, these details are lost when we sample points from generated spherical harmonics and are thus invisible in the pre-training.

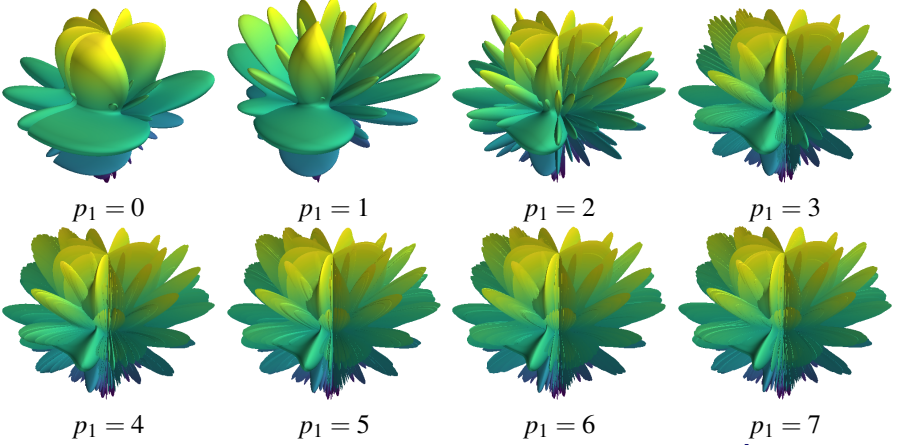


Figure 5: Impact of coefficient  $p_1$  in spherical harmonics. For all objects:  $[m_1, m_2, m_3, m_4] = [2, 1, 2, 2]$  and  $[p_2, p_3, p_4] = [2, 1, 2]$ .

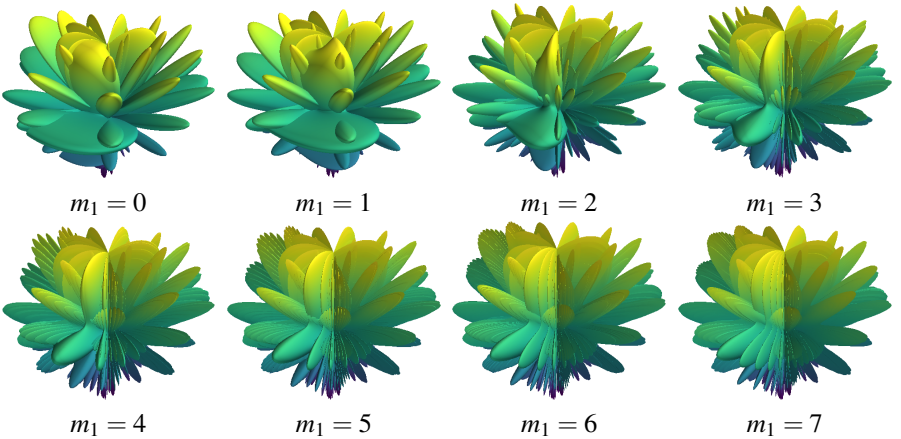


Figure 6: Impact of coefficient  $m_1$  in spherical harmonics. For all objects:  $[m_2, m_3, m_4] = [1, 2, 2]$  and  $[p_1, p_2, p_3, p_4] = [2, 2, 1, 2]$ .

The impact of the coefficients is illustrated in Fig. 5, where all coefficients are fixed except  $p_1$ . With increasing  $p_1$ , the ‘fins’ of the corresponding spherical harmonics become finer. A similar effect can be seen in Fig. 6, where the influence of  $m_1$  is visualized. With



large coefficients, the overall appearance of spherical harmonics is close to each other. Thus, we constrain the spherical harmonics in the low-frequency range to generate diverse scenes.

## B Pseudo Color in Pre-training

Dataset	Colors	mAcc	mIoU
From Scratch	-	66.4	60.0
RM-Harmonics	const.	69.8	62.8
RM-Harmonics	const. + DA	74.1	67.1
ScanNet	const.	69.8	63.6
ScanNet	const. + DA	73.1	67.0
ScanNet	real	74.7	67.6

Table 6: Impact of colors in pre-training using MAE. Fine-tuned for semantic segmentation on S3DIS dataset and evaluated in Area 5. The first two columns refer to the pre-training data. Const.: constant RGB values for all points. DA: data augmentation on color channels.

Since simulation and rendering are not involved, the scenes generated in this work don’t contain color information. However, color channels are crucial in some downstream tasks, *e.g.*, semantic segmentation. To transfer models trained on colorless point clouds to such tasks, we apply pseudo colors and data augmentation to color channels in pre-training. Specifically, we set all color channels to a constant value (*i.e.*, 0.5) and apply random color jitter to each point. Also, we simultaneously set color values of all points to 0 with the probability 0.5 (*i.e.*, color drop out).

Experiments are conducted to analyze the effect of this approach. We first pre-train an MAE on the RM-Harmonics dataset. As shown in Tab. 6, when no data augmentation (*i.e.*, jitter and drop out) is applied to color values, the constant pseudo color leads to significantly worse results with RM-Harmonics. Also, we pre-train the model on ScanNet and compare the performance of pseudo colors and real-world colors. Without data augmentation on pseudo colors, the performance in segmentation is much lower than using real-world colors. However, applying data augmentation significantly shrinks the gap. Interestingly, when both use pseudo colors, RM-Harmonics slightly outperforms ScanNet in pre-training. Results in Tab. 6 show that pseudo colors can be applied to pre-train models requiring colors on colorless point clouds. Also, data augmentation is essential for improving performance. We believe models learn color invariance via data augmentation and focus on the geometric information in the pre-training. In contrast, the color-dependent relationship is learned in fine-tuning where real-world colors are available.

## C Data Generation

We generate scenes based on the rules of Rao *et al.* [26]. Modifications are made to the original configurations. Our procedure can be summarized as follows:

1. Randomly pick 12 to 16 objects from the object set.
2. Independently apply data augmentation to each object (more details in Sec. D)

3. Sort the objects in descending order based on their projection areas on the horizontal plane (X-Y plane).
4. Randomly set the area (X-Y plane) of a rectangular room depending on the area sum of objects so that the objects can fit into the generated scene.
5. Randomly generate walls and floors according to the area.
6. Place each object by randomly choosing a position on the X-Y plane. Objects can be stacked on previous ones as long as the current height of the position is below 2 m. Otherwise, choose a new position.
7. For multi-view point clouds, voxelize the entire scene with voxel size 0.04 m. We further randomly sample 40000 points and save them for pre-training.
8. For single-view point clouds, randomly place a virtual camera in the scene and capture a depth map via ray-casting. Check the result so that each depth map contains at least 7 objects. All depth maps have the resolution  $640 \times 480$ , following the real-world dataset ScanNet [24]. The camera intrinsic and camera pose are also saved.

Since Rao *et al.* [26] didn't open source their code, our work is based on our implementation. Our code will be made publicly available.

## D Pre-processing and Data Augmentation

**In Data Generation.** Data augmentation is applied on each object during scene generation. Specifically, we first normalize an object into a unit sphere and randomly scale it with a factor uniformly distributed in  $[0.7, 1.5]$ . Then we flip the object left-right with a probability of 0.5 and rotate the object around the vertical axis (Z-axis) with an arbitrary angle. For spherical harmonics, we further swap Z-axis and Y-axis with the probability 0.5 since spherical harmonics show approximate rotational symmetry around Z-axis (see Tab. 5 and 6). We do so to prevent models from learning the bias that all objects are approximately symmetric around the vertical axis. At last, we randomly sample 3000 points from each object for generating multi-view point clouds. To generate single-view data via ray-casting, we use mesh representation without sampling.

**For Pre-training.** The primary pre-processing involved in our pipelines is cropping a region from an entire scene. However, the generated data must be differently pre-processed depending on pre-training methods and inputs:

1. For MAE with multi-view point clouds: we randomly choose a point in a complete point cloud and crop the closest 20000 points (*i.e.*, 50 %).
2. For MAE with single-view point clouds: we crop a rectangular region with a random ratio in  $[0.6, 0.8]$  from a depth map and transform the crop into a point cloud.
3. For contrastive learning: similar approaches are applied as for MAE. Specifically, we crop spherical regions in multi-view point clouds and crop depth maps for single-view point clouds. However, in each scene, we make two overlapping crops instead of one to create a positive pair for contrastive learning.

Subsequently, we apply standard data augmentation to each crop, including random translation, rotation around Z-axis, scaling, point jitter, and left-right flipping.

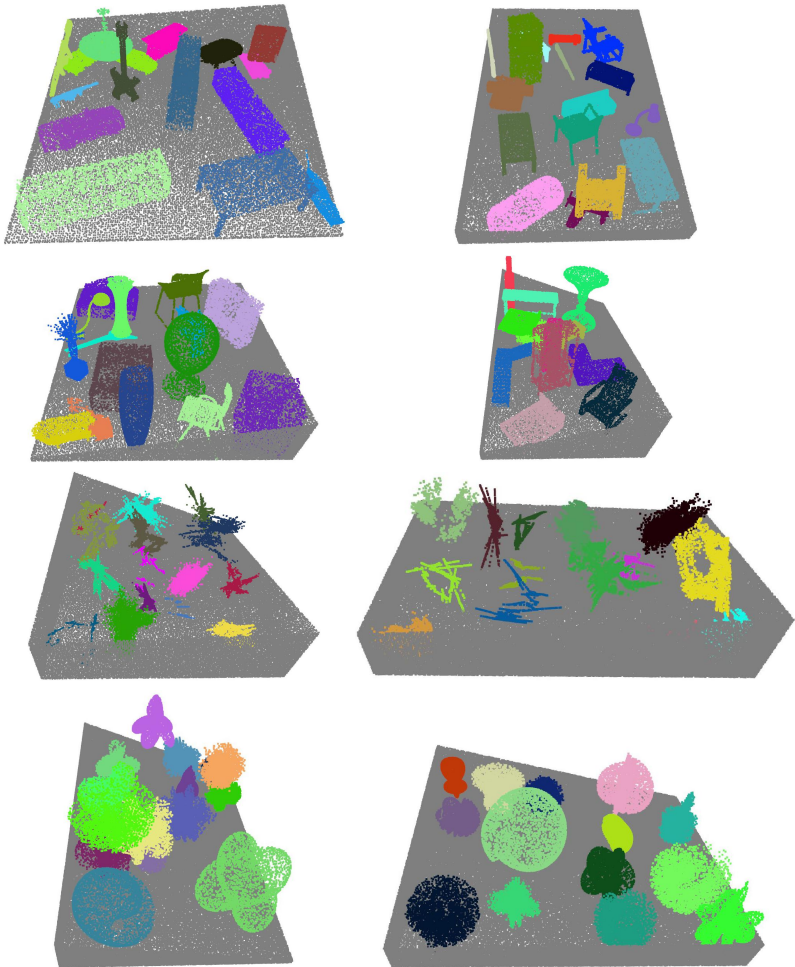


Figure 7: More examples of generated scenes. From the first to the fourth row: RM-ShapeNet, RM-ModelNet, RM-Fractal, and RM-Harmonics, respectively.

## E More Visualizations

We visualize more generated scenes in Fig. 7.